Journal of Applied Polymer Science

Extrusion foaming behavior of a polypropylene/nanoclay microcellular foam

Mingyi Wang,[1] Linsheng Xie,[1] Bo Qian,[1] Yulu Ma,[1] Nanqiao Zhou[2]

[1]School of Mechanical and Power Engineering, East China University of Science and Technology, Shanghai 200237, China
[2]Key Laboratory of Polymer Processing Engineering (Ministry of Education), National Engineering Research Center of Novel Equipment for Polymer Processing, South China University of Technology, Guangzhou 510640, China
Correspondence to: L. Xie (E-mail: clxw@ecust.edu.cn)

ABSTRACT: With maleic anhydride grafted polypropylene (PP-*g*-MAH) as a compatibilizer, composites of block-copolymerized polypropylene (B-PP)/nanoclay were prepared. The effects of the PP-*g*-MAH and nanoclay content on the crystallization and rheological properties of B-PP were investigated. The microcellular foaming behavior of the B-PP/nanoclay composite material was studied with a single-screw extruder foaming system with supercritical (SC) carbon dioxide (CO_2) as the foaming agent. The experimental results show that the addition of nanoclay and PP-*g*-MAH decreased the melt strength and complex viscosity of B-PP. When 3 wt % SC CO_2 was injected as the foaming agent for the extrusion foaming process, the introduction of nanoclay and PP-*g*-MAH significantly increased the expansion ratio of the obtained foamed samples as compared with that of the pure B-PP matrix, lowered the die pressure, and increased the cell population density of the foamed samples to some extent. © 2016 Wiley Periodicals, Inc. J. Appl. Polym. Sci. **2016**, *133*, 44094.

KEYWORDS: composites; extrusion; foams; nanoparticles; nanowires and nanocrystals; porous materials

Received 22 January 2016; accepted 16 June 2016
DOI: 10.1002/app.44094

INTRODUCTION

Polypropylene (PP), for which raw material is abundant, is cheap and easily processed. As such, PP has become one of the fastest developing general resins. Foamed PP material, which serves as an alternative to polystyrene in the packaging of food and electronics, has attracted more and more attention in the foam industry. However, compared with those of polystyrene and polyethylene, the processing window of PP for extrusion foaming is very narrow.[1] This makes the foaming process of PP extremely difficult to control. Therefore, it is difficult to produce PP foam products with a high expansion ratio and fine cell structure.

The addition of nanofiller in the microcellular foaming process of plastics, which induces heterogeneous nucleation, can provide a large number of nucleation sites; this improves the cell population density of the foam products.[2–7] Supercritical (SC) carbon dioxide (CO_2) is cheap, nontoxic, and nonflammable and does not leave remaining solvent in the foaming process of plastics. Thus, it creates no environmental pollution; this is consistent with the requirements of current green environmental protection policies. In this research, the extrusion foaming of block-copolymerized polypropylene (B-PP)/nanoclay composites assisted by SC CO_2 was studied to determine the effects of nanoclay on the foaming behavior of B-PP, and the underlying mechanism was clarified.

EXPERIMENTAL

Materials

The polymer matrix used in this study was a PP block copolymer (BA212E; Austrian Borealis Co., Vienna, Austria) with a melt flow rate (MFR) of 0.3 g/10 min (ISO 1133, 230 °C/2.16 kg). Nanoclay (Cloisite 20A; Southern Clay Products, Inc., Austin, TX) and maleic anhydride grafted polypropylene (PP-*g*-MAH; Epolene G-3003; America Eastman Chemical Co., Kingsport, TN) with an MFR of 360 g/10 min at 230 °C/2.16 kg were used as the nucleating agent and compatibilizer, respectively. SC CO_2 (Linde Co., Mississauga, Canada), with purity of 99.5%, was used as the foaming agent.

Sample Preparation

First, the B-PP, nanoclay, and PP-*g*-MAH used for the study were vacuum-dried at 80 °C for 8 h before use, and then, different concentrations of B-PP, nanoclay, and PP-*g*-MAH (as shown in Table I) were dry-blended in a high-speed mixing machine to obtain the B-PP/nanoclay premix. The premix was subsequently melt extruded with a twin-screw extruder (model D6/2, Brabender Co., Germany) to prepare pellets for extrusion foaming.

Table I. Compositions of the B-PP/PP-*g*-MAH/Nanoclay Composites and DSC Results

	Weight (%)					
Sample	B-PP	PP-*g*-MAH	Nanoclay	T_m (°C)	T_c (°C)	X_c (%)
1	100	0	0	167.76	130.13	44.27
2	98	1.5	0.5	167.28	130.52	45.24
3	96	3	1	167.56	129.67	43.78
4	88	9	3	166.90	131.04	45.06
5	80	15	5	166.73	130.6	43.34

w = weight.

The screw speed was 150 rpm; this resulted in an extrusion rate of 2.5 kg/h. The temperature profile in the twin-screw extruder barrel from the feeding zone to the die was kept at 190–200–210–210–220–220–200 °C for all blends. Extrusion foaming experiments were conducted on a single-screw extruder foaming system (05-25-000, Brabender) with a filament die; the die channel length was 1 mm, and the die diameter was 1.2 mm. The MFR of the extrudate from the die was kept at 13 g/min in the extrusion foaming process. The SC CO_2 content injected into the barrel was fixed at 3% (mass fraction) throughout the foaming process; it was accurately adjusted and regulated through the control of both the gas flow rate of the high-pressure syringe pump and the material feed rate. A single-phase polymer solution was achieved under the strong shear action of screw mixing and the static mixers. When the polymer/gas solution entered the filament die, it experienced a rapid pressure drop; this caused a sudden decrease in gas solubility in the polymer. Hence, a large number of bubbles were nucleated in the polymer matrix, and a foam structure was created; this was followed by bubble growth.[8] The foamed samples at various foaming temperatures were collected for characterization. The concentrations of each ingredient in the formula of the composites are listed in Table I.

Characterization

Differential scanning calorimetry (DSC; model 2910; TA Co., New Castle, DE) tests for all of the samples were carried out at a heating rate of 10 °C/min over a temperature range from 20 to 200 °C with nitrogen atmosphere protection. First, the sample was heated from 20 to 200 °C, held at 200 °C for 5 min to remove the thermal history, then cooled to 20 °C at a 10 °C/min cooling rate, and finally, reheated to 200 °C again. Data for cooling and the second heating cycle were recorded first, and then, the melting temperature (T_m) and crystallization temperature (T_c) values for the B-PP matrix and the B-PP/PP-*g*-MAH/nanoclay blends were read from the graphs, as listed in Table I. The crystallinity percentage (X_c) of the neat PP and PP in its nanocomposites determined by DSC are also included in Table I. X_c of the PP phase was calculated according to eq. (1):

$$X_c = \frac{\Delta H_f}{\Delta H_f^o} \times 100 \quad (1)$$

where ΔH_f is the normalized enthalpy of fusion per gram of the sample in the second heating scan measured at the T_m and ΔH_f^o is the melting enthalpy of 100% crystalline PP and was equal to 207 J/g.[9]

To investigate the clay dispersion and exfoliation, B-PP/PP-*g*-MAH/nanoclay composite pellets were hot-pressed at 210 °C to make a film for X-ray diffraction analysis. Wide-angle X-ray diffraction (WAXD) tests were conducted on an X-ray diffractometer (model D8 Advance, Bruker Corp., Germany). A Cu Kα radiation source with a wavelength of 1.5406 Å was used by the detector.

A high-pressure capillary rheometer (Rheologic 5000, Ceast Corp., Italy) with a drawing acceleration of 2.5 mm/s^2 was used to determine the tensile melt strength of the B-PP matrix and the corresponding B-PP/PP-*g*-MAH/nanoclay composites.

Dynamic shearing rheological properties tests for the B-PP and B-PP/PP-*g*-MAH/nanoclay composites were conducted on a strain-controlled ARES rheometer with a 25-mm parallel-plate geometry and a 1-mm sample gap. Dynamic shear measurements with frequencies from 0.1 to 70 Hz were taken at a temperature of 210 °C with nitrogen atmosphere protection. The strain was maintained at 10% to ensure linear viscoelasticity.

The density of the foamed samples was determined with the buoyancy method. For details of the method, see ref. [10]. Scanning electron microscopy (SEM) was used to characterize the cell morphology of the foamed samples. All of the foamed samples were dipped into liquid nitrogen and quickly fractured in air before scanning. Then, the fractured cross sections of the samples were sputter-coated with platinum in a sputter coater (Polaron SC7620, Quorum Technologies Companies, East Sussex, United Kingdom). The cell size and cell population density were determined by SEM micrographs. We calculated the cell diameter by averaging the sizes of at least 100 cells from the SEM micrographs. For details of the methods used to calculate the cell population density of the foamed samples, see ref. [11].

RESULTS AND DISCUSSION

DSC Testing

As shown in Table I, the T_m values of all of the composites were lower than that of the pure B-PP, whereas the T_c values of the composites were higher than that of the pure B-PP, except for sample 3, in which T_c was slightly lower than that of the pure B-PP. The changing trend of the T_c values of the B-PP/PP-*g*-MAH/nanoclay composites was similar to that of the LH-PP/nanoclay composites studied in our previous research,[12] in which the underlying mechanism was clarified. As such, T_c was affected by the PP-*g*-MAH and nanoclay content in the composites. It is also shown in Table I that PP in samples 2 and 4 had

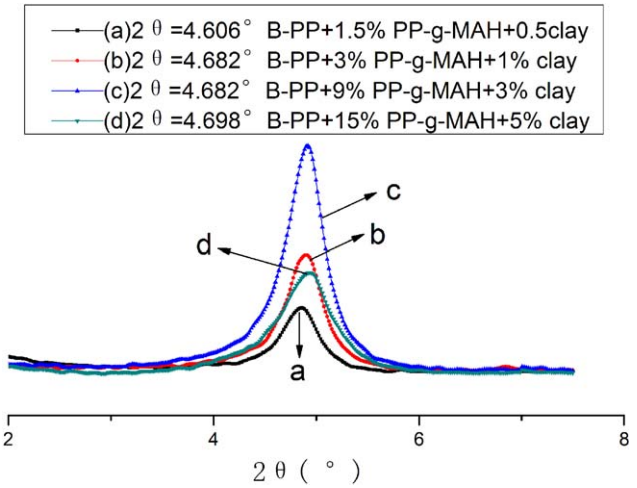

Figure 1. WAXD patterns for the B-PP/PP-*g*-MAH/nanoclay composites. [Color figure can be viewed in the online issue, which is available at wileyonlinelibrary.com.]

a slightly higher crystallinity than the neat PP, and this appeared to be due to the higher nucleating effect in these composites. In contrast, PP in samples 3 and 5 had slightly a lower crystallinity than the neat PP; this might have been due to the hindrance of the polymer chain diffusion by clay particles.[13]

WAXD

The WAXD patterns for the B-PP/PP-*g*-MAH/nanoclay composites are shown in Figure 1. The layer spacing for the organically modified nanoclay was $d_0 = 2.42$ nm, and the corresponding diffraction angle 2θ was 3.648°. After melt intercalation, as the nanoclay contents in the B-PP/PP-*g*-MAH/nanoclay composites were 0.5, 1, 3, and 5 wt %, the diffraction angles (2θs) corresponding to the first characteristic peak of nanoclay were 4.606, 4.682, 4.682, and 4.698°, respectively; this indicated that the diffraction angle shifted to a larger angle. Thus, the corresponding layer spacing for nanoclay in the B-PP/PP-*g*-MAH/nanoclay composites decreased compared with that for the nanoclay before melt intercalation. Again, with the increase in the nanoclay content in the composites, the layer spacing showed a tendency to decrease. Two possible reasons might explain the contraction of the nanoclay layer spacing in the composites. On the one hand, this might have been caused by the high viscosity of B-PP used for the research; this made the macromolecular chain of B-PP difficult to insert into the nanoclay layers. On the other hand, a cation-exchange reaction might have occurred in the blending process, and some alkyl ammonium cations were replaced; this would have resulted in decreased layer spacing.

Table II. Melt Strength Values of the B-PP/PP-*g*-MAH/Nanoclay Composites

	Weight (%)			Melt strength (cN)
Sample	B-PP	PP-*g*-MAH	Nanoclay	
1	100	0	0	13.9
2	98	1.5	0.5	12.4
3	96	3	1	11.45
4	88	9	3	6.9
5	80	15	5	8.41

w = weight.

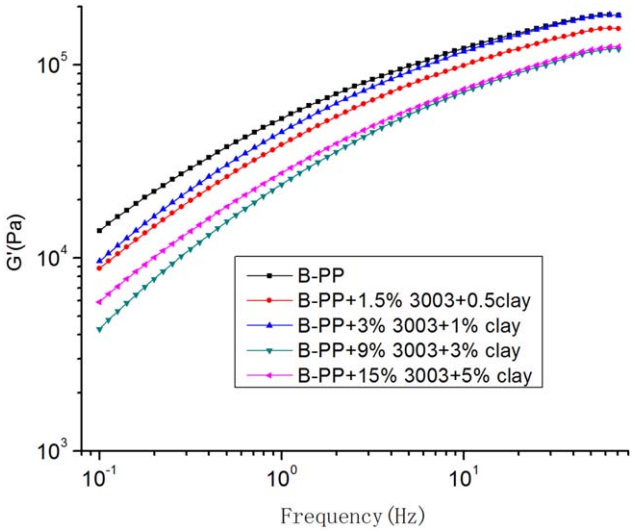

Figure 2. Storage modulus (G') values of the B-PP and B-PP/PP-*g*-MAH/nanoclay composites. [Color figure can be viewed in the online issue, which is available at wileyonlinelibrary.com.]

Rheologic Property Testing

The tensile melt strength values of the B-PP/PP-*g*-MAH/nanoclay composites at 190 °C are listed in Table II. As shown in Table II, compared with pure B-PP, the tensile melt strength of the B-PP/PP-*g*-MAH/nanoclay composites decreased, and with increasing nanoclay and PP-*g*-MAH contents in the composites, the tensile melt strength of the composites decreased initially and then increased because the addition of nanoclay increased the melt strength of the composites, whereas the addition of PP-*g*-MAH with a high MFR reduced the viscosity and the

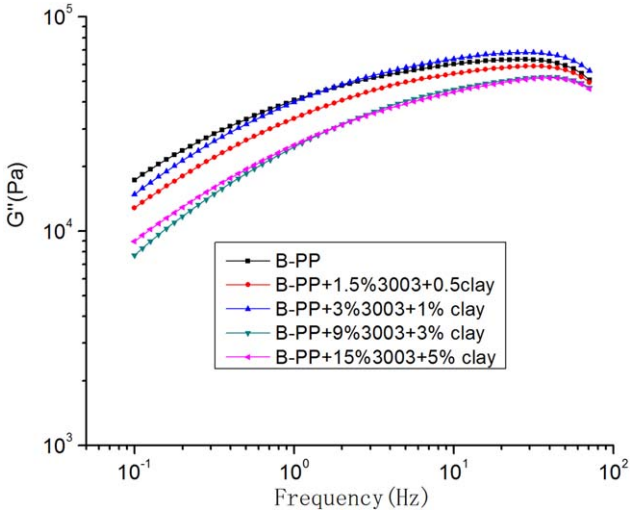

Figure 3. Loss modulus (G') values of the B-PP and B-PP/PP-*g*-MAH/nanoclay composites. [Color figure can be viewed in the online issue, which is available at wileyonlinelibrary.com.]

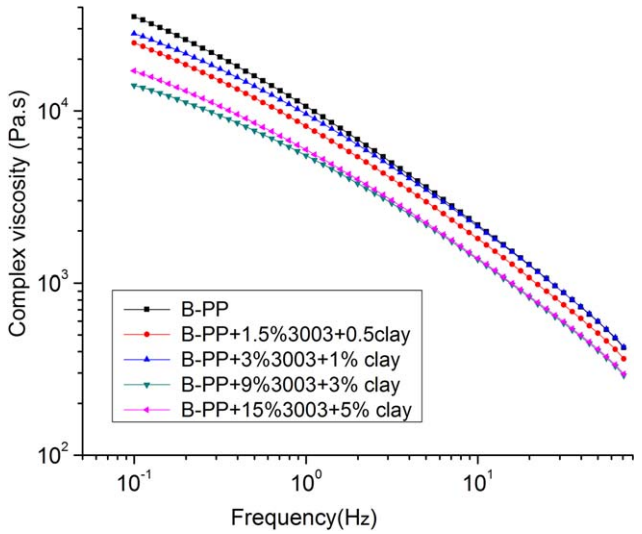

Figure 4. Complex viscosity values of the B-PP and B-PP/PP-*g*-MAH/nanoclay composites. [Color figure can be viewed in the online issue, which is available at wileyonlinelibrary.com.]

corresponding melt strength of the composites. With increasing nanoclay and PP-*g*-MAH contents in the composites, the nanoclay or PP-*g*-MAH may have become the dominant factor influencing the melt strength and caused the melt strength to increase or decrease.

The variance of the sample storage and loss moduli within the scanning frequency range is presented in Figures 2 and 3. The addition of nanoclay and PP-*g*-MAH decreased the storage and loss moduli of the blends system; this might have been due to the high MFR of PP-*g*-MAH used in this study. Figure 4 shows the complex viscosity values of the B-PP and B-PP/PP-*g*-MAH/nanoclay composites; they indicated that the addition of nanoclay and PP-*g*-MAH decreased the complex viscosity of the composites, which showed a similar changing trend as the tensile melt strength shown in Table II. The results might have been based on the following mechanism. Generally, the addition of nanoclay can make the complex viscosity of composites increase, whereas the addition of PP-*g*-MAH with a high MFR can reduce the complex viscosity of composites. With the variance of the nanoclay and PP-*g*-MAH contents in the composites, nanoclay or PP-*g*-MAH may have become the dominant factor influencing the complex viscosity, and this might have caused the complex viscosity of the composites to increase or decrease.

Effects of the Die Temperature and Formulation on the Expansion Ratios of the Foam Products Obtained from the B-PP/PP-*g*-MAH/Nanoclay Composites

As shown in Figure 5, when the injected SC CO_2 content was 3 wt % relative to the pure B-PP matrix, the addition of nanoclay and PP-*g*-MAH significantly increased the maximum expansion ratio of the foamed samples from the B-PP/PP-*g*-MAH/nanoclay composites. This was based on the fact that because the SC CO_2 content was low, the introduction of nanoclay and PP-*g*-MAH provided more nucleation sites and caused more gas to be used for bubble nucleation and growth. The heterogeneous nucleation was the main mechanism determining the cell population density and foaming expansion ratio. In addition, the presence of nanoparticles may have hindered CO_2 diffusion by creating a more tortuous diffusive pathway.[14] Another phenomenon, as shown in Figure 3, was that at a lower foaming temperature (160 °C), the expansion ratio of the foam products from the pure B-PP matrix decreased significantly, whereas the expansion ratio of the foam products from the B-PP/PP-*g*-MAH/nanoclay composites did not decrease as much. This finding might have been due to the lower T_m of the composites compared with that of the pure B-PP matrix; this could have delayed the decrease in the expansion ratio for the foam products caused by skin hardening at a low foaming temperature.

Figure 6 shows the micrographs of cross sections of the foam samples from the pure B-PP matrix and B-PP/PP-*g*-MAH/nanoclay composites with a mass ratio of 80:15:5 at different foaming temperatures. As shown in Figure 6, compared with that of the pure B-PP matrix, the cell size of the foam samples from the B-PP/PP-*g*-MAH/nanoclay composites was larger, and the cell wall became thinner; this might have been caused by the decreased viscosity and melt strength of the composites as compared with those of the pure B-PP matrix.

Effects of the Die Temperature and Formulation on the Cell Population Density of the Foam Products Obtained from the B-PP/PP-*g*-MAH/Nanoclay Composites

Figure 7 shows the influence of the die temperature and formulation on the cell population density of the foamed samples. Overall, when the SC CO_2 content was 3 wt %, the introduction of nanoclay and PP-*g*-MAH increased the cell population density of the foam products from the B-PP/PP-*g*-MAH/nanoclay composites as compared with those from the pure B-PP matrix,

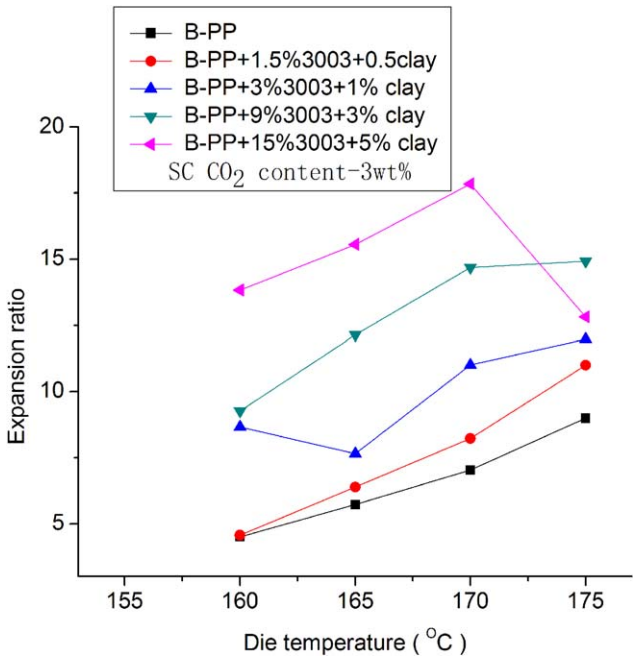

Figure 5. Effect of the die temperature and blend ratio on the expansion ratio of the foam products obtained from the B-PP/PP-*g*-MAH/nanoclay composites. [Color figure can be viewed in the online issue, which is available at wileyonlinelibrary.com.]

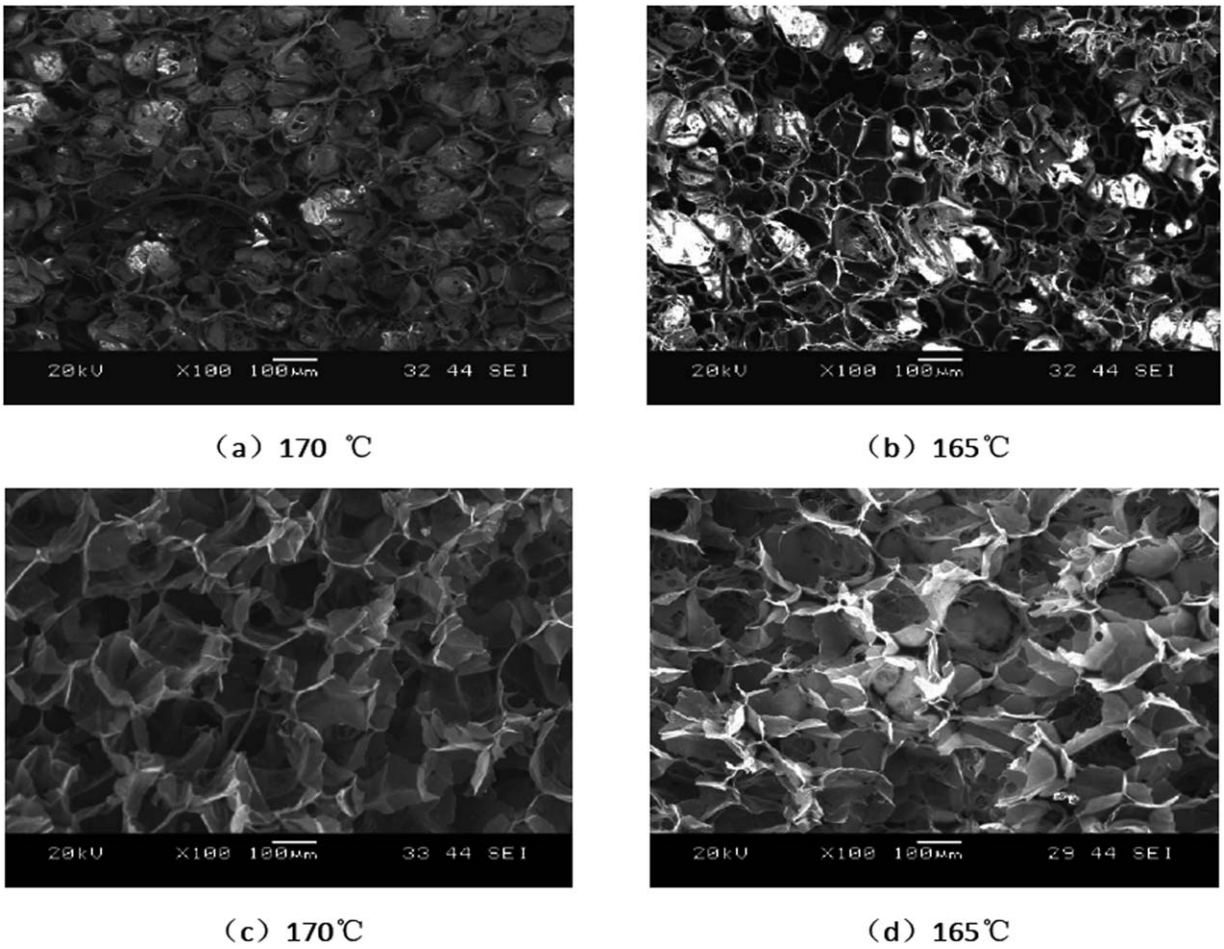

Figure 6. Cell morphology of the (a,b) foamed B-PP and (c,d) foamed B-PP/PP-*g*-MAH/nanoclay composites with a mass ratio of 80:15:5.

but the improvement was not apparent because the introduction of nanoclay and PP-*g*-MAH triggered heterogeneous nucleation and, thus, provided a large number of nucleation sites. This increased the cell population density. In contrast, the addition of nanoclay and PP-*g*-MAH decreased the complex viscosity and melt strength of the composites compared with the pure B-PP matrix; this resulted in a loss of gas used for bubble nucleation. The final cell population density was the result of competition between the previous two mechanisms.

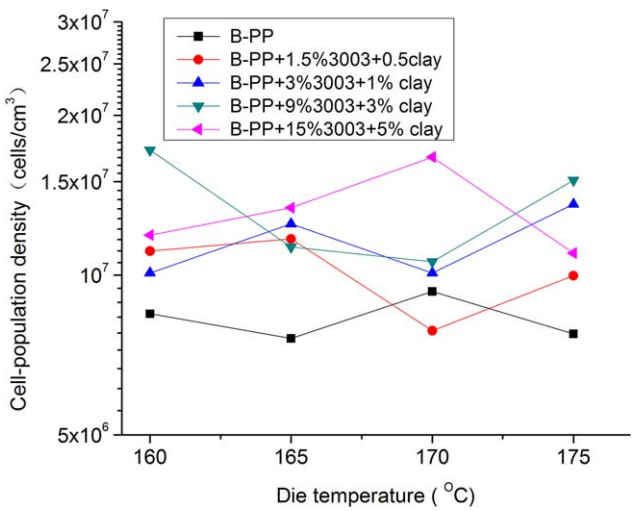

Figure 7. Effect of the die temperature and blend ratio on the cell population density of the foam products obtained from the B-PP/PP-*g*-MAH/nanoclay composites. [Color figure can be viewed in the online issue, which is available at wileyonlinelibrary.com.]

CONCLUSIONS

In this study, the extrusion foaming of B-PP with and without the addition of nanoclay with SC CO_2 as the foaming agent was investigated to determine the effects of the formulation and foaming temperature on the cell morphology, expansion ratio, and cell population density of the obtained foam products. The key conclusions from our research are as follows:

1. Compared with those of the pure B-PP, the tensile melt strength and shearing complex viscosity of the B-PP/PP-*g*-MAH/nanoclay composites decreased, and with increasing nanoclay and PP-*g*-MAH contents in the composites, the tensile melt strength and shearing complex viscosity of the B-PP/PP-*g*-MAH/nanoclay composites decreased and then increased when a minimum value was reached.
2. When the content of SC CO_2 used as the foaming agent was 3 wt %, the addition of nanoclay and PP-*g*-MAH

significantly increased the maximum expansion ratio of the foamed samples from the B-PP/PP-*g*-MAH/nanoclay composites compared with the pure B-PP matrix.

3. The introduction of nanoclay and PP-*g*-MAH increased the cell population density of the B-PP/PP-*g*-MAH/nanoclay composites as compared with that of the pure B-PP matrix, but the improvement was not apparent.

ACKNOWLEDGMENTS

This work was financially supported by the National Natural Science Foundation of China (contract grant number 21206152) and the Beijing Natural Science Foundation (contract grant number 3132007).

REFERENCES

1. Burt, J. G. *J. Cell. Plast.* **1978**, *4*, 341.
2. Okamoto, M.; Nam, P. H.; Maiti, P.; Kotaka, T.; Nakayama, T.; Takada, M.; Ohshima, M.; Usuki, A.; Hasegawa, N.; Okamoto, H. *Nano Lett.* **2001**, *1*, 503.
3. Nam, P. H.; Maiti, P.; Okamoto, M.; Kotaka, T.; Nakayama, T.; Takada, M.; Oshima, M.; Usuki, A.; Hasegawa, N.; Okamoto, H. *Polym. Eng. Sci.* **2002**, *42*, 1907.
4. Wang, M. Y.; Ji, L. Q.; Chu, R.; Park, C. B.; Zhou, N. Q. *Cell. Polym.* **2011**, *30*, 227.
5. Jiang, X. L.; Bao, J. B.; Liu, T.; Zhao, L.; Xu, Z. M.; Yuan, W. K. *J. xsCell. Plast.* **2009**, *45*, 515.
6. Marcelo, A.; Jose, I. V.; Vera, R.; Eusebio, S. *Polym. Eng. Sci.* **2009**, *49*, 2400.
7. Zheng, W. G.; Lee, Y. H.; Park, C. B. *J. Appl. Polym. Sci.* **2010**, *117*, 2972.
8. Zhai, W. T.; Park, C. B.; Kontopoulou, M. *Ind. Eng. Chem. Res.* **2011**, *50*, 7282.
9. Abadchi, M. R.; Jalali-Arani, A. *Iran. Polym. J.* **2015**, *24*, 805.
10. Wang, M. Y.; Ma, J.; Chu, R.; Park, C. B.; Zhou, N. Q. *J. Appl. Polym. Sci.* **2012**, *123*, 2726.
11. Baldwin, D. F.; Park, C. B.; Suh, N. P. *Polym. Eng. Sci.* **1996**, *36*, 1437.
12. Wang, M. Y.; Ji, L. Q.; Ma, J.; Zhou, N. Q. *Polym. Mater. Sci. Eng.* **2011**, *27*, 114.
13. Hegde, R. R.; Bhat, G. S.; Spruiell, J. E.; Benson, R. *J. Polym. Res.* **2013**, *20*, 1.
14. Keshtkar, M.; Nofar, M.; Park, C. B.; Carreau, P. J. *Polymer.* **2014**, *55*, 4077.